Inclusive measurements of electromagnetic dissociation of ^{197}Au targets

T. Aumann, J. V. Kratz, and E. Stiel
Institut für Kernchemie, Universität Mainz, D-6500 Mainz, Germany

K. Sümmerer, W. Brüchle, M. Schädel, and G. Wirth
Gesellschaft für Schwerionenforschung, D-6100 Darmstadt, Germany

M. Fauerbach
Institut für Kernphysik, Technische Hochschule Darmstadt, D-6100 Darmstadt, Germany

J. C. Hill
Iowa State University, Ames, Iowa 50011
(Received 3 August 1992)

Cross sections for the electromagnetic dissociation of ^{197}Au targets by 1.7 GeV/nucleon ^{20}Ne and 1 GeV/nucleon ^{86}Kr, ^{197}Au, and ^{209}Bi beams have been measured by an activation method. We observe systematic discrepancies between the experimental data and a simple Weizsäcker-Williams calculation: For the heaviest projectiles, the calculation overpredicts the $1n$ cross sections, whereas the $2n$ and $3n$ cross sections are systematically underpredicted. The deviations can be significantly reduced, however, by calculations including isoscalar and isovector giant quadrupole excitations as well as the possibility to excite multiphonon states. The most important experimental result of the present study is the observation of large cross sections for three-neutron removal from ^{197}Au with ^{197}Au and ^{209}Bi projectiles which can only be explained by a dominant contribution from two-phonon giant dipole excitation. For an almost quantitative reproduction for all xn channels observed, we have to assume a higher excitation probability by roughly a factor of 2 for the double giant dipole resonance as compared to the harmonic approach.

PACS number(s): 24.30.Cz, 27.80.+w

I. INTRODUCTION

In a series of target-inclusive experiments at the Berkeley Bevalac, Mercier *et al.* and Hill *et al.* [1] have studied the electromagnetic dissociation (ED) of ^{59}Co, ^{89}Y, and ^{197}Au targets by relativistic projectiles ranging from ^{12}C to ^{139}La with energies between 1.26 and 2.1 GeV/nucleon. Qualitative agreement was found between measured cross sections for the one-neutron- and two-neutron-emission channels and a simple Weizsäcker-Williams (WW) calculation [2]. Quantitatively, however, systematic deviations between the results of the WW calculations and the data were observed: For a gold target, e.g., the ED part of the experimental $1n$-removal cross section is larger than the theoretical value for ^{20}Ne projectiles with an energy of about 2 GeV/nucleon, whereas for ^{139}La projectiles at 1.26 GeV/nucleon the experimental value is below the WW calculation. If scaled to the same bombarding energy (assuming the WW theory gives the correct bombarding-energy dependence of the ED cross sections) the experimental cross sections for a gold target could be reproduced by a power law, $\sigma_{\rm exp} \sim Z_{\rm proj}^{1.56\pm0.04}$, whereas $\sigma_{\rm WW} \sim Z_{\rm proj}^{1.85}$. Given these results, it seemed to be worthwhile to perform similar studies at the new SIS heavy-ion synchrotron at GSI, Darmstadt, with even heavier projectiles than ^{139}La to see if the rather large discrepancies expected for large values of $Z_{\rm proj}$ could be verified experimentally. After this work was completed, Hill *et al.* [3] have published cross sections for the reaction ^{197}Au(^{238}U, $1n$)^{196}Au at 0.96 GeV/nucleon bombarding energy.

Another objective of the present experiment was the search for indications of multiphonon excitations of the giant dipole resonance (GDR). Bertulani and Baur [4] have shown that multiphonon GDR states can be excited with large probabilities in relativistic heavy-ion collisions. As has been pointed out by Llope and Braun-Munzinger [5,6], SIS energies of the order of 1 GeV/nucleon are particularly well suited to search for such effects in heavy systems due to a relative suppression of single-phonon GDR excitations. Since higher-order GDR excitations are expected to contribute mainly to the emission of more than one neutron, we have measured the $2n$ cross section for 1 GeV/nucleon ^{197}Au + ^{197}Au, and $3n$ cross sections for 1 GeV/nucleon ^{86}Kr, ^{197}Au, and ^{209}Bi + ^{197}Au. To clearly distinguish higher-order ED from first-order effects, we have performed WW calculations including both isoscalar and isovector giant quadrupole excitations as well as multiphonon excitations following the approach of Llope and Braun-Munzinger [5, 6]. As will be shown in Sec. IV of this paper, we can reproduce our results for the $1n$, $2n$, and $3n$ channels simultaneously only if we include a strong second-order GDR excitation.

 ©1993 The American Physical Society

II. EXPERIMENTAL PROCEDURE AND RESULTS

A. Beam intensity measurements

The experimental procedure used in the present experiment is very similar to the one extensively discussed in the work of Hill *et al.* [1]. It consists of irradiating gold targets with relativistic heavy ions between ^{20}Ne and ^{209}Bi and a determination of the cross section for the formation of $^{194-196}$Au by observing the γ-ray activity following β decay of these reaction products. As can be seen from Table I, which contains the essential information on the bombardments performed, most of our experiments were done at 1 GeV/nucleon bombarding energy. The beams of ^{20}Ne, ^{86}Kr, ^{197}Au, and ^{209}Bi were delivered from the SIS synchrotron with intensities ranging between 10^9 particles per spill for ^{20}Ne (experiment A) and 3×10^5 particles per spill for experiments B, C, and E. A separate bombardment with a gold beam of higher intensity (experiment D) was performed to measure the $2n$ cross section relative to the $1n$ cross section. In all cases the spill length was adjusted to about 1 sec with a repetition rate of typically one per 10 sec.

In the three experiments with low beam intensities (B, C, and E) the numbers of projectiles hitting the targets were counted with two plastic scintillation detectors ($10 \times 10 \times 0.1$ mm^3), one before the first of the three targets, the other behind the last target. In order to be able to correct for secondary reactions in the targets [1], in these three runs three 1×1 cm^2 targets with different thicknesses were bombarded simultaneously. The targets were displaced by about 5 cm distance from each other to minimize cross talk. The number of ions hitting the first and the last target were taken as the number of counts in the upstream and downstream scintillators, respectively. For the center target, the average of the scintillator counts was taken. The differences in the count rates were always less than 5%.

The high beam intensities in experiment A were monitored with an absolutely calibrated secondary-electron emission detector [7]. Position measurements of the beam with multiwire chambers made sure that the beam spot on the target was always smaller than the width of the targets. In addition, the target was cut into pieces which were measured separately. Thus the intensity distribution on the target could be checked to make sure that the whole beam intensity was seen by the target. In the case of experiment D, only the time variation of the beam intensity was monitored, whereas the absolute normalization of the number of incident ^{197}Au ions was determined with the help of the formation cross section of ^{196}Au measured in experiment C.

B. Gamma-ray spectroscopy of the induced activity

The residual γ-ray activities of ^{196}Au and ^{194}Au in the targets were measured with calibrated Ge detectors, following the decay curves for several half-lives. For the experiments B, C, and E with total beam intensities of about 10^9 incident particles a close detector geometry was needed. Therefore, corrections for coincidence summing in the detector were necessary to determine the yield of the residual products ^{196}Au and ^{194}Au. These corrections amounted to about 10% in both cases. Self-absorption in the targets and fluctuations of beam intensity during the bombardments were also taken into account to evaluate the activities at the end of irradiation.

The activity of ^{195}Au, which decays with a half-life of 183 d, emitting γ rays of 99 keV only, was measured with a low-energy Ge detector during a period of about 100 d. The measured value was corrected for self-absorption in the target based on well-known mass absorption coefficients and an experimental simulation using an inactive Au foil of the same thickness and a radioactive source (about 60% correction). Corrections for coincidence summing with x rays (about 5%) and interfering γ lines (<5%) were also taken into account.

C. Cross section determination

From the activities determined as described above the experimental cross sections for the $1n$, $2n$, and $3n$ channels have been calculated using the measured target thicknesses and numbers of incident beam particles. As is usual in the case of target-activation experiments, these cross sections have to be corrected for contributions from secondary reactions induced mainly by evaporation neutrons. The number of neutrons produced in the target is proportional to the target thickness, and the correction for these reactions can be performed by measuring the cross sections as a function of target thickness and

TABLE I. Irradiation parameters for the irradiation of ^{197}Au targets by various projectiles used in the present experiment.

Experiment	Projectile	Energy (GeV/nucleon)	Integrated flux (particles)	Target thicknesses (mg/cm^2)
A	^{20}Ne	1.7	1.7×10^{12}	58
B	^{86}Kr	1.0	1.0×10^{9}	58,120,193
C	^{197}Au	1.0	1.1×10^{9}	58,120,193
D	^{197}Au	1.0	6.3×10^{10}	203
E	^{209}Bi	1.0	6.8×10^{8}	58,116,193

TABLE II. Experimental and theoretical cross sections for one-neutron removal from a ^{197}Au target. The nuclear cross sections $\sigma_{\rm nucl}^{\rm expt}$ are indirectly determined cross sections from Refs. [1, 3] using factorization, while $\sigma_{\rm nucl}^{\rm calc}$ are from our intranuclear-cascade calculations. The calculated ED cross sections $\sigma_{\rm ED}^{\rm calc}$ include single-phonon GQR and multiphonon GDR excitation as described in the text.

Proj.	Energy (GeV/nucleon)	$\sigma_{\rm tot}^{\rm expt}$ (mb)	Corr. sec. react. (%)[a]	$\sigma_{\rm nucl}^{\rm expt}$ (mb)	$\sigma_{\rm nucl}^{\rm calc}$ (mb)	$\sigma_{\rm ED}^{\rm expt}$ (mb)	Ref.	$\sigma_{\rm ED}^{\rm calc}$ (mb)
^{12}C	2.1	178±7	5	103±12	79	75±14	[1]	46
^{20}Ne	1.7	242±13	8.3		91	151±13	This expt.	111
^{20}Ne	2.1	268±11	7.2	115±12	91	153±18	[1]	119
^{40}Ar	1.8	463±30	5	115±15	110	348±34	[1]	322
^{56}Fe	1.7	707±52	5	106±14	122	601±54	[1]	614
^{86}Kr	1.0	958±62	4.1		138	820±62	This expt.	868
^{139}La	1.26	2130±120	1	160±30	160	1970±130	[1]	2062
^{197}Au	1.0	3255±200	1.0		178	3077±200	This expt.	3151
^{209}Bi	1.0	3425±205	1.5		181	3244±205	This expt.	3399
^{238}U	0.96	3440±210		280±90	188	3160±230	[3]	3890

[a]The correction for secondary reactions applies to the thinnest target in the respective experiments.

extrapolating to zero target thickness. This was done for the $1n$ and $3n$ cross sections. The correction for the cross section of experiment A with ^{20}Ne as the projectile was taken from Ref. [1]. The corrections applied to the measured cross sections for the thinnest target in the respective experiment (58 mg/cm^2 for this work) are listed in column 4 of Tables II and IV for the $1n$ and $3n$ channels, respectively. In case of the $2n$ channel (experiment D), where only one target (200 mg/cm^2) could be measured, we assumed that the relative yield of ^{195}Au due to secondary processes is intermediate between those for the $1n$ and $3n$ channels. For a 200 mg/cm^2 target and 1 GeV/nucleon ^{197}Au as the projectile, these corrections are 3.4% for the $1n$ and 25% for the $3n$ channel. Taking the average, we correct the $2n$-out cross section by 14% and assume an error of ±10%. The resulting experimental cross sections, $\sigma_{\rm tot}^{\rm exp}$, which are corrected for contributions from secondary reactions, are listed in column 3 of Tables II–IV.

The measured cross sections $\sigma_{\rm tot}^{\rm exp}$ represent the sum of nuclear and ED processes leading to the observed fragments $^{194-196}$Au. To isolate the ED part of the cross section, the nuclear contribution has to be subtracted. Hill *et al.* [1] have measured various ^{197}Au(RHI,Y)X cross sections (X representing various targetlike spallation products with suitable decay characteristics and RHI representing a relativistic heavy ion) and deduced the nuclear ^{197}Au(RHI,xn)$^{197-x}$Au cross sections by appropriately scaling the measured ^{197}Au(p,xn)$^{197-x}$Au cross sections by the ratio $\sigma[^{197}{\rm Au}({\rm RHI},Y)X]/\sigma[^{197}{\rm Au}(p,Y)X]$ [1]. The numbers, $\sigma_{\rm nucl}^{\rm exp}$, are given in column 5 of Tables II and III for the $1n$ and $2n$ cross sections.

As an independent approach to the nuclear part of the measured cross sections—which allows us also to calculate the respective values for the $3n$ channel—we have performed intranuclear-cascade (INC) calculations with the ISABEL code [8]. As can be seen from Fig. 1, these calculations reproduce with good accuracy the measured $1n$ to $3n$ cross sections for high-energy protons impinging on ^{197}Au targets [1, 9] where the ED part can be neglected. For heavier projectiles, the calculated nuclear cross sections show the expected $A_{\rm proj}^{1/3}$ dependence, represented by the solid line in Fig. 1. As can be seen from Figs. 1(a) and 1(b), the values obtained by the scaling procedure of Ref. [1] for the $1n$ and $2n$ channels agree with our calculated values within ±50% (dashed lines in Fig. 1).

As further evidence for the validity of our INC calculations we note that our measured total $3n$ cross sections

TABLE III. Same as Table II for two-neutron removal from a ^{197}Au target.

Projectile	Energy (GeV/nucleon)	$\sigma_{\rm tot}^{\rm expt}$ (mb)	Corr. sec. react. (%)[a]	$\sigma_{\rm nucl}^{\rm expt}$ (mb)	$\sigma_{\rm nucl}^{\rm calc}$ (mb)	$\sigma_{\rm ED}^{\rm expt}$ (mb)	Ref.	$\sigma_{\rm ED}^{\rm calc}$ (mb)
^{40}Ar	1.8	141±15		65±10	48	76±18	[1]	45
^{56}Fe	1.7	133±9		60±9	49	73±13	[1]	85
^{139}La	1.26	424±47		89±18	55	335±49	[1]	275
^{197}Au	1.0	701±105	14		58	643±105	This expt.	414

[a]The correction for secondary reactions applies to a target thickness of 203 mg/cm^2 (see text).

TABLE IV. Cross sections for three-neutron removal from a ^{197}Au target. The nuclear cross sections $\sigma_{\rm nucl}^{\rm calc}$ are from our intranuclear-cascade calculations. The calculated ED cross sections $\sigma_{\rm ED}^{\rm calc}$ include single-phonon GQR and multiphonon GDR excitation as described in the text.

Projectile	Energy (GeV/nucleon)	$\sigma_{\rm tot}^{\rm expt}$ (mb)	Corr. sec. react. (%)[a]	$\sigma_{\rm nucl}^{\rm calc}$ (mb)	$\sigma_{\rm ED}^{\rm expt}$ (mb)	$\sigma_{\rm ED}^{\rm calc}$ (mb)
^{20}Ne	1.7	40.5±4.0	19	37	3.5±4.0	2.0
^{86}Kr	1.0	71±16	16	51	20±16	16
^{197}Au	1.0	233±26	7	62	171±26	94
^{209}Bi	1.0	283±28	5	62	221±28	106

[a]The correction for secondary reactions applies to a target thickness of 58 mg/cm^2.

for 1.7 GeV/nucleon ^{20}Ne and 1 GeV/nucleon ^{86}Kr projectiles, which give an upper limit for the nuclear cross section with only a small ED contribution, lie within the error band in Fig. 1(c). The agreement with the full curve in Fig. 1(c) gets even better when we apply the usual corrections to the raw data. In case of the ^{20}Ne $3n$ cross section from experiment D we have to correct only for secondary reactions, since the ED part is calculated to amount only to 2 mb, half the size of the error bar. Since only one target thickness has been used in experiment D, we have to extrapolate secondary contributions deduced for Kr, Au, and Bi projectiles as described above and assume that the flux of secondary particles scales with the geometrical cross section. We obtain a contribution of 9 mb from secondary processes. (In column 3 of Table IV the corrected value for $\sigma_{\rm tot}^{\rm exp}$ is given.) In Fig. 1(c) the total cross section without correction is represented by the full square, the correction described above is indicated by the arrow. For the ^{86}Kr $3n$ cross section

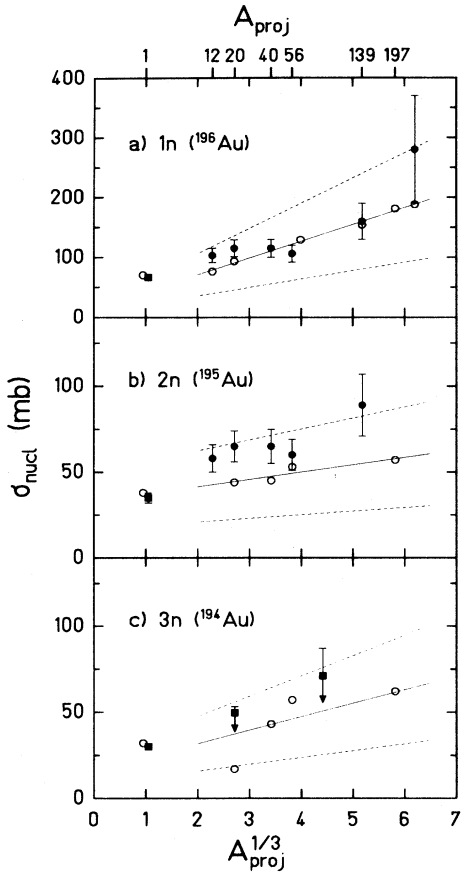

FIG. 1. Nuclear $1n$-out to $3n$-out cross sections for ^{197}Au targets as a function of projectile nuclear mass, $A_{\rm proj}$. The full squares represent experimentally determined cross sections for protons [1, 9] and upper limits for experiments with ^{20}Ne and ^{86}Kr (this work), respectively. The full circles have been obtained by scaling the proton-induced data by Hill *et al.* [1, 3] (see text). The open circles are results from our intranuclear-cascade (INC) calculations. The solid lines have been fitted to the INC values assuming an $A_{\rm proj}^{1/3}$ dependence. The dashed lines indicate a ±50 % error attributed conservatively to the calculated nuclear cross sections.

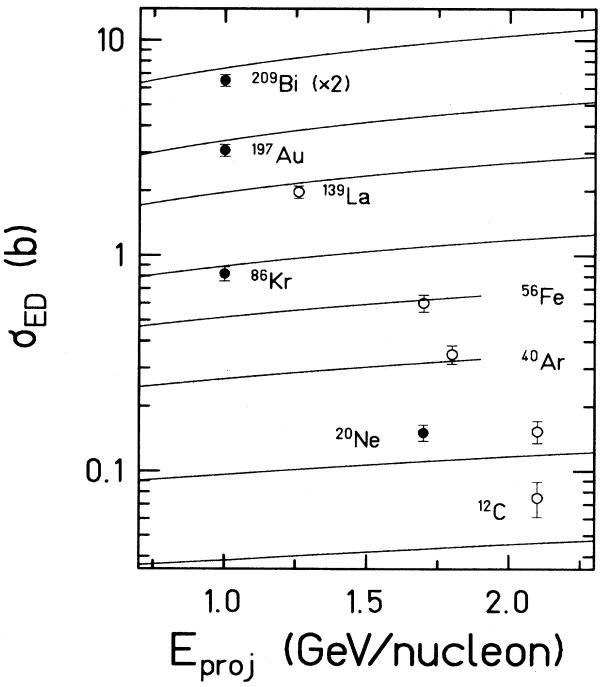

FIG. 2. Experimental ED cross sections for one-neutron removal from a ^{197}Au target for various projectiles as a function of projectile energy compared to simple WW calculations without multiphonon excitations (full lines). The open circles are from Ref. [1], the full points are from this work.

(where the secondary correction has been performed exactly as discussed at the beginning of this subsection) the ED contribution is somewhat larger (16 mb according to our calculations, indicated by the arrow) but still of magnitude similar to the experimental error.

We list the nuclear cross sections from our INC calculation in column 6 of Tables II and III for the $1n$ and $2n$ channels, respectively, and in column 5 of Table IV for the $3n$ channel. These numbers were used in this work to subtract the nuclear contribution from the measured total cross section, $\sigma_{\rm tot}^{\rm exp}$, to obtain the experimental ED cross sections, $\sigma_{\rm ED}^{\rm exp}$, listed in columns 7 and 6 of Tables II–IV, respectively. For completeness, we list in Tables II and III also the ED cross sections from Ref. [1] obtained by subtracting the experimental nuclear cross sections, $\sigma_{\rm nucl}^{\rm exp}$.

The large ED cross sections that result for the heaviest projectiles—which are of prime interest for the present study—give confidence that the remaining uncertainties in the determination of the nuclear cross sections are negligible. Even if we allow for an error of $\pm 50\%$ for the nuclear contribution indicated by the dashed lines in Fig. 1, this uncertainty is about as large as the experimental errors discussed above. The situation is different, however, for light projectiles. This will be discussed in more detail in Sec. IV. Figure 2 shows our experimental ED cross sections for the $1n$ channel as a function of projectile energy, together with the Bevalac data [1]. The curves represent simple WW calculations described in the following section.

III. CALCULATION OF ELECTROMAGNETIC DISSOCIATION CROSS SECTIONS

The usual procedure to calculate cross sections for the ED process is the WW method [2, 4] of virtual quanta. In this approach, the cross section is given by integrating over the product of the equivalent photon number $N_\gamma(E_\gamma)$ and the photonuclear cross section $\sigma_\gamma(E_\gamma)$:

$$\sigma_{\rm ED} = \int dE_\gamma N_\gamma(E_\gamma)\sigma_\gamma(E_\gamma). \quad (1)$$

At ultrarelativistic energies, the photon numbers $N_\gamma(E_\gamma)$ are equal for different multipolarities, therefore the experimental photoabsorption cross sections, $\sigma_\gamma^{\rm exp}(E_\gamma)$, can be used in Eq. (1). At intermediate energies, however, the number spectra of equivalent photons are different for different multipolarities [4]. As an example, the upper part of Fig. 3 shows the spectra for equivalent $E1$ and $E2$ photons for the case of ^{197}Au + ^{197}Au at 1 GeV/nucleon, indicating that $E2$ photons are more abundant at this energy than $E1$ photons. As a consequence, it is necessary to break up $\sigma_\gamma^{\rm exp}(E_\gamma)$ into different components corresponding to different multipolarities. Under the assumption that only $E1$ and $E2$ contribute to the measured photonuclear cross section, Norbury [10] has calculated the dipole contribution $\sigma^{E1}(E_\gamma)$ from the relation

$$\sigma^{E1}(E_\gamma) = \sigma_\gamma^{\rm exp}(E_\gamma) - \sigma_{\rm IS}^{E2}(E_\gamma), \quad (2)$$

where $\sigma_{\rm IS}^{E2}(E_\gamma)$ represents the theoretical quadrupole

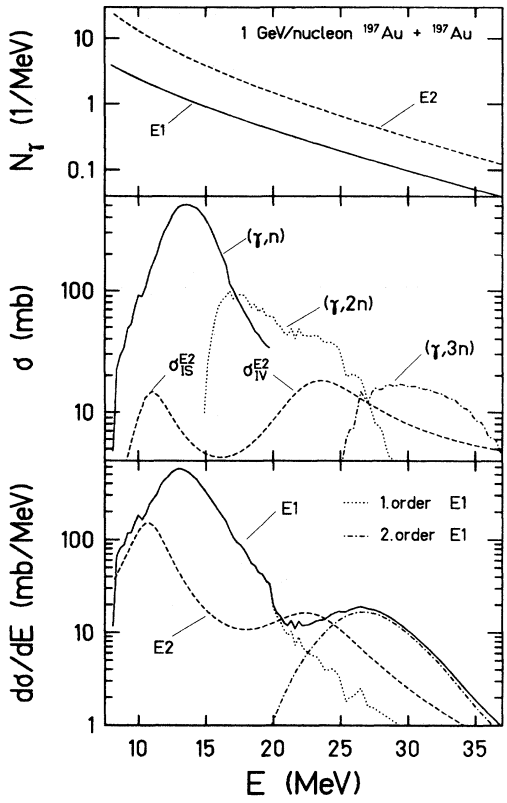

FIG. 3. Top: Equivalent $E1$ and $E2$ photon spectra for 1 GeV/nucleon ^{197}Au + ^{197}Au. Middle: Experimental photonuclear cross sections from Ref. [12] for one-neutron emission (full curve) and for two-neutron emission (dotted curve). The dot-dashed curve for the $3n$ emission has been obtained in a compound-nucleus decay calculation with the code HIVAP [14]. To indicate the influence of giant quadrupole excitation (GQR), the Lorentzian curves for isoscalar (IS) and isovector (IV) GQR (dashed curve) are indicated. The Lorentzian parameters are given in Table V. Bottom: Differential cross sections for GDR and GQR excitations. For the GDR component, first-order and second-order contributions are indicated separately by the dotted and dash-dotted lines, respectively.

cross section calculated with a Lorentzian parametrization of the isoscalar part of the giant quadrupole resonance (GQR) taken from the literature. We follow Norbury's procedure but take into account also the isovector GQR cross section, $\sigma_{\rm IV}^{E2}(E_\gamma)$, to obtain

$$\sigma^{E1}(E_\gamma) = \sigma_\gamma^{\rm exp}(E_\gamma) - [\sigma_{\rm IS}^{E2}(E_\gamma) + \sigma_{\rm IV}^{E2}(E_\gamma)]. \quad (3)$$

Parameters for the GQR in ^{197}Au were extracted from the review of Bertrand *et al.* [11] and are listed in Table V. The middle part of Fig. 3 shows the GQR strength distribution according to this parametrization together with the experimental (γ, n)- and $(\gamma, 2n)$-excitation functions [12]. The bottom part of this figure shows that a multiplication of the GQR strength with the $E2$ equivalent photon spectrum leads to significant contributions of the isoscalar GQR to the $1n$, and of the isovector GQR to the $2n$ channel, respectively.

TABLE V. Lorentzian parameters of the isoscalar (IS) and isovector (IV) giant quadrupole resonance in ^{197}Au as extracted from the work of Bertrand *et al.* [11].

	Resonance energy (MeV)	Resonance width (FWHM) (MeV)	Sum rule strength (%)
IS	10.8	2.9	95
IV	23.0	7.0	95

Since in our measurements we have examined different xn-emission channels, we have to rewrite Eq. (1) separately for each channel:

$$\sigma_{\mathrm{ED},xn} = \sum_{L=E1,E2} \int dE_\gamma N_\gamma^L(E_\gamma)\sigma_\gamma^L(E_\gamma) f_{xn}(E_\gamma), \tag{4}$$

where $f_{xn}(E_\gamma)$ is the fraction of the photonuclear cross section leading to the respective xn channel. For x=1,2, $f_{xn}(E_\gamma)$ can be read off the graphs in Ref. [12]. (We have multiplied the experimental photonuclear cross sections for ^{197}Au from Ref. [12] by a factor of 0.93 as suggested by Berman *et al.* [13].) Since the absorption of real photons on ^{197}Au has been measured only up to 27 MeV photon energy, no direct experimental information is available for the $(\gamma, 3n)$-excitation function. This channel is very sensitive, however, to the strength of the two-phonon GDR excitation, as will be shown later. We have therefore deduced the $f_{3n}(E_\gamma)$ values from compound-nucleus decay calculations with the code HIVAP [14]. The resulting $(\gamma,3n)$ excitation function is also shown in the middle panel of Fig. 3. The validity of this approach has been verified by observing that the calculated f_{1n} and f_{2n} values follow closely those from the experiment [12]. For excitation energies between 27 MeV and 50 MeV, the Lorentzian with the fitted parameters from Ref. [12] was taken as the total photoabsorption cross section, and the fraction $f_{3n}(E)$ for evaporating three neutrons was determined from the HIVAP calculation as described above.

Another important input quantity for the WW calculations is the minimum impact parameter, $b_{\min}$, below which nuclear processes dominate over electromagnetic ones. Like Hill *et al.* [1], we have first used the Benesh-Cook-Vary (BCV) parametrization [15],

$$b_{\min} = r_0[A_{\mathrm{proj}}^{1/3} + A_{\mathrm{target}}^{1/3} - X(A_{\mathrm{proj}}^{-1/3} + A_{\mathrm{target}}^{-1/3})], \tag{5}$$

with r_0=1.34 fm and X=0.75.

Alternatively, we have tested the parametrization of Kox *et al.* [16],

$$b_{\min} = r_0\left(A_{\mathrm{proj}}^{1/3} + A_{\mathrm{target}}^{1/3} + a\frac{A_{\mathrm{proj}}^{1/3}A_{\mathrm{target}}^{1/3}}{A_{\mathrm{proj}}^{1/3} + A_{\mathrm{target}}^{1/3}} - c\right), \tag{6}$$

with r_0=1.1 fm, a=1.85, and c=1.9. This formula has been developed for a very good overall description of interaction cross sections between heavy nuclei at medium and high energies. As will be discussed in more detail in Sec. IV, this choice of $b_{\min}$ gives a better reproduction of experimental $1n$ ED cross sections and is therefore favored compared to Eq. (5).

Performing the WW calculations using Eq. (4) with $b_{\min}$ from Eq. (6), $1n$-removal cross sections, $\sigma_{\mathrm{ED},1n}$, have been obtained which are shown in Fig. 2 together with the experimental data of this work and that of Hill *et al.* [1]. Irrespective of the different projectile energies of the various experiments, it is obvious from Fig. 2 that for reactions of the type ^{197}Au(RHI,$1n$)^{196}Au the WW calculations are in good agreement with the data only for ^{40}Ar and ^{56}Fe projectiles. For lighter projectiles, our WW calculations always underestimate the cross sections, whereas for heavier projectiles they are appreciably overestimated. The latter discrepancies could result from the absorption of several photons in a collision, leading to the excitation of multiphonon GDR states, as suggested previously [4, 5]. We have therefore adopted the method of Llope and Braun-Munzinger [5, 6] of calculating multiple GDR excitations in the harmonic approximation in the framework of a WW calculation [4]. (Contributions from multiple GQR excitations are much smaller than the errors of our data and can therefore safely be neglected.) According to Ref. [5] we obtain for the differential cross section in first order

$$\frac{d\sigma^{(1)}}{dE} = \int_{b_{\min}}^{\infty} db\, 2\pi b\, P^{(1)}(b) q^{(1)}(E,b), \tag{7}$$

where $P^{(1)}(b)$ is the probability to absorb exactly one photon in a collision with impact parameter b,

$$P^{(1)}(b) = m_\gamma(b) e^{-m_\gamma(b)}, \tag{8}$$

and $q^{(1)}(E,b)$ is the probability that the photon absorbed in this collision has an energy of E:

$$q^{(1)}(E,b) = \frac{N_\gamma(E,b)\sigma_\gamma(E)}{m_\gamma(b)}. \tag{9}$$

In both equations, $m_\gamma(b)$ denotes the mean number of photons absorbed in one collision,

$$m_\gamma(b) = \int dE_\gamma N_\gamma(E_\gamma, b)\sigma_\gamma(E_\gamma). \tag{10}$$

The cross section for an xn channel is obtained to first order by integrating Eq. (7) over energy with the factor $f_{xn}(E)$ inserted as in Eq. (4):

$$\sigma_{\mathrm{ED},xn}^{(1)} = \int\int dE\, db\, 2\pi b\, e^{-m_\gamma(b)}\, N_\gamma(E,b)\sigma_\gamma(E) f_{xn}(E). \tag{11}$$

In a similar way the corresponding equations for the absorption of exactly two and three photons can be derived [5]. The calculations were done up to third order, where the third order, however, can be neglected. In this approach the excitation energy of the two-phonon GDR is about twice the excitation energy of the GDR, and also the width is about twice the width of the GDR, spanning the excitation-energy region leading to the evaporation

TABLE VI. Comparison between experimental and calculated $1n$, $2n$, and $3n$ cross sections for the reaction ^{197}Au(^{197}Au,xn)$^{197-x}$Au at 1 GeV/nucleon. The theoretical cross sections in parentheses have been obtained with an enhancement factor $f_{\mathrm{DGDR}} = 2.2$ for the two-phonon GDR as explained in the text.

Exit channel	Experimental cross section (mb)	Calculated cross sections (mb) No multiple excitation			With multiple excitation		
		Total	GDR	GQR	Total	First order GDR	Second order GDR
$1n$	3077±200	3414	2866	548	3151 (2836)	2603 (2287)	0.4 (0.9)
$2n$	643±105	377	263	114	414 (459)	235 (201)	66 (145)
$3n$	171±26	30	8	22	94 (171)	7 (6)	65 (143)
Sum ($1n$ - $3n$)	3891±227	3821	3137	684	3659 (3466)	2845 (2494)	131 (289)

of two and three neutrons. Apart from a factor $e^{-m_\gamma(b)}$, Eq. (11) is identical to the normal WW calculation [Eq. (4)]. This means that the cross sections calculated to first order, $\sigma_{\mathrm{ED}}^{(1)}$, are smaller than those calculated with the simple WW calculation neglecting multiphonon absorption if the mean number of absorbed photons is high. Since only first order contributes to the $1n$ channel, this leads to a reduced $1n$ cross section, while the $2n$ and $3n$ channels are increased by second-order excitation. The bottom part of Fig. 3 shows that the $3n$ channel is most sensitive to two-phonon GDR excitation, whereas for the $2n$ channel GQR and second-order GDR are of similar magnitude. More quantitatively, the different contributions are listed separately in Table VI for the reaction ^{197}Au(^{197}Au,xn)$^{197-x}$Au at 1 GeV/nucleon.

Adding the $E1$ cross sections for multiphoton absorption to the $E2$ cross sections obtained as described above, the theoretical cross sections listed in the last columns of Tables II–IV have been obtained. Qualitatively, similar discrepancies as noted above in the context of the simple WW calculation without multiple-photon absorption persist. The magnitude of these deviations has been reduced considerably, however. The calculated $2n$ and $3n$ cross sections, e.g., for ^{197}Au + ^{197}Au, are lower than the experimental values, in contrast to the observation made for the $1n$ channel, where the calculated cross sections are larger than the experimental ones. We will discuss this more quantitatively in the following section.

IV. DISCUSSION

The experiments described in this paper and those of other authors [1,3] have been performed at different bombarding energies dictated by the available beams from the SIS and Bevalac accelerators. From the comparison presented in Fig. 2 we conclude that the discrepancies between our calculations and the experimental data depend systematically on the projectile charge and not on the bombarding energy. For a more detailed comparison, we feel therefore free to remove the incident-energy dependence of the ED cross sections by scaling the measured cross sections according to the WW prescription (including second-order GDR and first-order GQR excitations). Figure 4 shows the experimental data of Tables II–IV

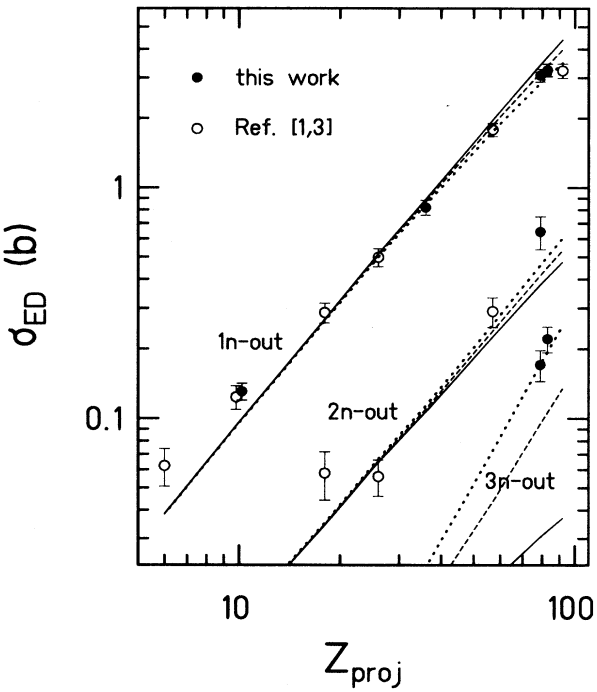

FIG. 4. ED cross sections for $1n$, $2n$, and $3n$ removal from a ^{197}Au target as a function of projectile charge. All experimental data points are scaled to the same bombarding energy of 1 GeV/nucleon. The full curve represents a simple WW calculation taking single-phonon GDR and GQR excitations into account. The dashed curve has been obtained by allowing for multiphonon GDR excitations in the harmonic approach. The dotted curve represents a calculation where the two-phonon GDR excitation probability is arbitrarily increased by a factor of 2.2.

scaled to the same projectile energy of 1 GeV/nucleon as a function of projectile charge number, $Z_{\rm proj}$. Also included in Fig. 4 are theoretical calculations with the WW formalism. The full curves do not take into account the possibility to absorb several $E1$ photons in one collision leading to higher-order GDR excitations [Eq. (4)], whereas the dashed and dotted curves include this contribution [Eq. (11)]. It is obvious that the experimental $1n$-out cross sections exhibit a smaller slope than the calculated ones. For the experimental $2n$-out cross sections, however, the situation is reversed: our value for the ^{197}Au(^{197}Au,$2n$)^{195}Au reaction is 70% above the simple WW calculation, the error bar of this data point being only 16%. For the $3n$ cross sections the deviations from the full curve become dramatic: The experimental cross sections for ^{197}Au and ^{209}Bi exceed the simple WW prediction by a factor of 5.7 and 6.8, respectively. We will demonstrate below, however, that the WW theory nevertheless forms an adequate basis to consistently reproduce our data almost quantitatively when multi-phonon excitations are properly taken into account.

A. One-neutron removal channels

We would like to discuss first how well we can reproduce the $1n$ ED cross sections, since these data are most abundant and have a higher accuracy compared to the $2n$ and $3n$ cross sections. For low-Z (^{12}C and ^{20}Ne) projectiles, we find an excess of cross section compared to WW theory (which is exaggerated, however, in magnitude compared to the substantial deficit for high-Z projectiles by the logarithmic scale in Fig. 4). As will be shown later, it is easy to conceive physical processes that lead to a reduction of the ED strength in the $1n$ channel for large $Z_{\rm proj}$ compared to a simple WW calculation. It is difficult, however, to find physical reasons why $\sigma_{\rm WW}$ should grossly *underestimate* the data. We are therefore tempted to attribute the excess cross section found in Fig. 4 for ^{12}C and ^{20}Ne projectiles to an insufficient knowledge of the nuclear contribution to the total $1n$ cross section. This would imply that both our intranuclear-cascade calculations and the factorization approach in Ref. [1] underestimate the nuclear $1n$ cross section for light projectiles. While it is difficult, if not impossible, to experimentally verify these speculations, we will in the following focus on the high-Z data, where the nuclear contribution is about equal in magnitude to the accuracy of the data points, so that our conclusions concerning the ED process are not very much affected by an insufficient knowledge of the nuclear part of the cross section.

Compared to the ED calculations of Hill *et al.* [1], our calculated $1n$ cross sections using the same simple WW theory without multiphonon excitations are somewhat larger due to our inclusion of GQR excitations. This leads to improved agreement for ^{40}Ar and ^{56}Fe projectiles, but to larger discrepancies for heavier projectiles. Table VI shows for the example of ^{197}Au + ^{197}Au at 1 GeV/nucleon, that in our calculation the excitation of the GQR contributes 548 mb or about 16% to the population of the $1n$-out channel. Including both $E1$ and $E2$ excitations in a simple WW calculation without multiphonon excitations leads to an overestimation of the $1n$ cross section by more than 10% in this reaction.

It has been noted in the preceding section that the inclusion of higher-order GDR excitations results in a lowering of the calculated $1n$-out cross sections (where the excitation of exactly one photon contributes most) while increasing those of other xn channels. The dashed curves in Fig. 4 represent these calculations with $E1$ excitations included up to third order, where the third order is negligible. As can be seen more quantitatively from comparison of columns 7 and 9 in Table II, the agreement with experiment is now very good for all projectiles between ^{40}Ar and ^{209}Bi. The remaining deviations from the experimental data, though within the error limits, indicate a small but systematic overprediction of the ED cross section by theory. We will come back to this point in the following section.

B. Two- and three-neutron removal channels

The most significant achievement of the present experiment has been the measurement of rather precise values for the $2n$- and $3n$-out cross sections for ^{197}Au + ^{197}Au and the $3n$-out cross section for ^{209}Bi + ^{197}Au. (The $3n$ cross sections obtained with ^{20}Ne and ^{86}Kr as projectiles and listed in the first two rows of Table IV are only insignificantly larger than the estimated nuclear contribution.) As can be seen from Fig. 4, the experimental $2n$ and $3n$ cross sections for heavy projectiles are grossly underestimated by the simple WW calculation. The somewhat better agreement of the data for the reaction ^{139}La(^{197}Au, $2n$)^{195}Au with our simple WW calculation compared to the calculations of Hill *et al.* [1] is once more due to the inclusion of the GQR, especially of the isovector GQR in this case. As can be seen qualitatively from the bottom panel in Fig. 3 and quantitatively from Table VI for the case of ^{197}Au + ^{197}Au, about 30% of the $2n$ cross section is from GQR excitation.

Figure 4 demonstrates that especially the magnitude of the $3n$ ED cross section is a sensitive measure of the strength of higher-order GDR excitations: the simple WW calculation (full curve) can only account for 18% of the measured value in the case of ^{197}Au + ^{197}Au, whereas the inclusion of the two-phonon GDR excitation can explain 55% of the observed cross section (dashed curve). It is obvious, however, that there remains still a rather large discrepancy. We are tempted to attribute this discrepancy to an enhancement of the two-phonon GDR excitation strength compared to the harmonic oscillator model underlying our calculations: our data call for a *decrease* of the $1n$ cross sections and an *increase* of the $2n$ and $3n$ cross sections for large $Z_{\rm proj}$ which is obtained easily by increasing the two-phonon GDR strength. This idea is corroborated by a recent result obtained by the LAND collaboration [17] for the double-GDR excitation in ^{136}Xe: There, a total two-phonon GDR cross section of 175±50 mb has been measured, compared to a theoretical estimate of 110 mb [6]. In order to introduce as little bias as possible in an estimate of a possible double-GDR enhancement factor, $f_{\rm DGDR}$, we plot in Fig. 5 the difference between our measured $1n$ to $3n$ cross sections

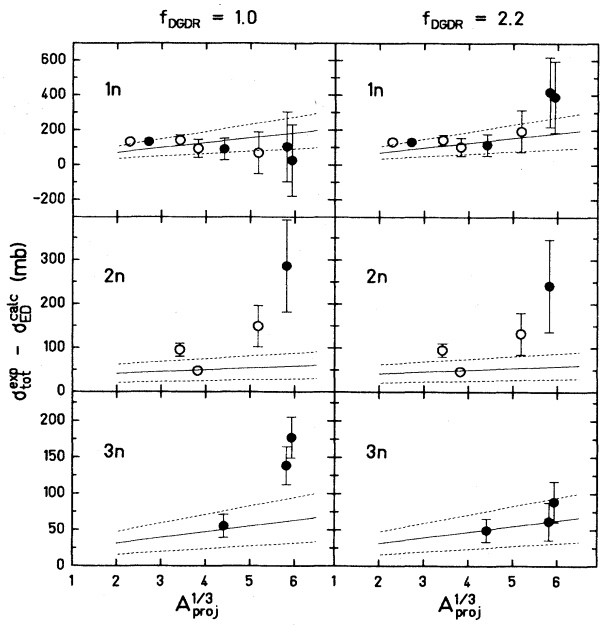

FIG. 5. Deviations between measured total cross sections for $1n$ to $3n$ removal from ^{197}Au and calculated values from WW theory for electromagnetic dissociation. The symbols have the same meaning as in Fig. 2. These deviations are compared to estimates of the nuclear contribution to the respective cross sections (see Fig. 1). The left column of panels represents a WW calculation with two-phonon GDR excitations in the harmonic approach. The right column shows the same calculation, but with the two-phonon GDR strength enhanced by a factor of 2.2, which minimizes the rms deviation between the data points and the full lines simultaneously for all channels. In all cases, the cutoff parameter, b_{min}, has been chosen as in Eq. (6) (Ref. [16]).

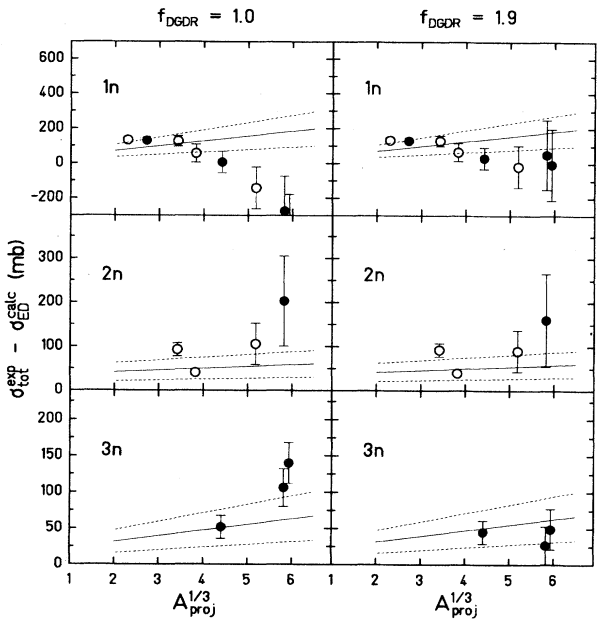

FIG. 6. Same as Fig. 5, but with a cutoff parameter, b_{min}, according to the Benesh-Cook-Vary parametrization [Eq. (5), Ref. [15]].

and the theoretical ED cross sections calculated for different values of f_{DGDR}. These differences represent "experimental" nuclear cross sections which—according to our discussion in Sec. II C—should lie within the dashed lines duplicated from Fig. 1. The upper left panel in Fig. 5 clearly shows that $f_{DGDR} = 1$ (no enhancement) would imply a continuous decrease in σ^{1n}_{nucl} when going from ^{12}C to ^{209}Bi projectiles, in contrast to an expected increase with $A^{1/3}_{proj}$. At the same time, the nuclear $2n$ and $3n$ cross sections would have to be much larger than the $1n$ cross sections and grossly exceed the estimates from Fig. 1. The right-hand column of Fig. 5 visualizes the differences between total experimental and calculated ED cross sections that result if we minimize simultaneously for all three channels the rms deviation of σ_{nucl} from the INC calculation, yielding $f_{DGDR} = 2.2 \pm 0.2$. With the exception of the $2n$ channel, the resulting nuclear part lies well within the expectations.

In Fig. 6, we finally want to demonstrate that the choice of b_{min} according to Eq. (5) as used in Refs. [1, 3, 6] is worse than that of Eq. (6). In particular, the calculated $1n$ cross sections are much too large. For $f_{DGDR} =$ 1, they exceed the measured total cross sections for large Z_{proj} implying negative values for σ_{nucl}. Even for the χ^2 minimum of the deviations of σ^{calc}_{nucl} from $\sigma^{exp}_{tot} - \sigma^{calc}_{ED}$, which is obtained for $f_{DGDR} = 1.9 \pm 0.2$, the values for σ^{1n}_{nucl} (top right panel in Fig. 6) barely exceed zero for the heaviest projectiles. (At the same time, we obtain somewhat better results for the $2n$ channel, which we consider less significant, however, than the $1n$ and $3n$ channels.) We note that for $b_{min} = 1.2(A^{1/3}_{proj} + A^{1/3}_{target})$ as used in Refs. [4, 5] the calculated $1n$ cross sections are even larger than for the BCV parametrization, again exceeding the experimental total $1n$ cross sections for all projectiles heavier than krypton.

V. SUMMARY AND CONCLUSIONS

The results of the present study extend the systematics of ED cross sections for ^{197}Au target dissociation towards higher projectile charge numbers. Calculations with the Weizsäcker-Williams theory of virtual photons can reproduce the measured cross sections with good accuracy, if the contributions from GQR excitation and from two-phonon GDR excitation are taken into account. We suggest to perform the WW calculations with a cutoff parameter, b_{min}, that has been found to reproduce measured interaction cross sections between heavy nuclei very well. We have shown that the remaining discrepancies between theory and experiment (too large predicted cross sections for the $1n$ channel and too low predictions for the $2n$ and $3n$ channels) can be resolved consistently by assuming a two-phonon GDR excitation probability that is roughly a factor of 2 larger than in the harmonic

approach. This finding is in line with similar observations made with the LAND neutron detector for the ED of ^{136}Xe. The factor of 2 enhancement of the two-phonon GDR excitation as compared to the harmonic approximation signals that the excitation probabilities for $\sim$ 1 GeV/nucleon ^{197}Au and ^{209}Bi beams have become so large that single- and multiple-phonon excitations can no longer be treated as independent processes. The data call for a theoretical treatment using coupled channels.

Within the precision reached with the present experiment it is difficult to give a precise value for the enhancement factor, since this value depends somewhat on the precise location, width, and strength of the isovector GQR, on the choice of the cutoff impact parameter, $b_{\min}$, of the WW calculation, and on a more accurate estimate of the nuclear contribution, which is difficult, if not impossible, to obtain. We want to emphasize, however, that the enhancement by roughly a factor of 2 corresponds to a stable χ^2 minimum in the reproduction of the calculated nuclear cross sections not only for the "best" choice of $b_{\min}$, but also for a quite different prescription for this parameter.

It will be interesting to see if the conclusions drawn from the inclusive measurements performed in the present study are corroborated by exclusive measurements of ^{208}Pb projectile dissociation studied presently with the LAND detector at GSI. Further information, in particular with respect to the GQR, could be gained if the same inclusive experiments would be performed at lower bombarding energies where the $E2$ equivalent photon spectrum is enhanced compared to the present experiments at higher energies.

ACKNOWLEDGMENTS

The authors are indebted to Dr. R. S. Simon for supplying an irradiated gold target for one of our measurements. We thank E. Schimpf and E. Jäger for their excellent technical assistance during all stages of the experiments and the GSI target laboratory for preparing gold targets. This work was supported by the German Minister for Research and Technology (BMFT) under Contract No. 06 MZ 106. One of us (J.C.H.) acknowledges the support of the U.S. Department of Energy under Contract No. DE-FG02-92ER40692 and also wishes to thank the North Atlantic Treaty Organization for travel support under a Collaborative Research Grant.

[1] M.T. Mercier, J.C. Hill, F.K. Wohn, C.M. McCullough, M.E. Nieland, J.A. Winger, C.B. Howard, S. Renwick, D.K. Matheis, and A.R. Smith, Phys. Rev. C **33**, 1655 (1986); J.C. Hill, F.K. Wohn, J.A. Winger, M. Khayat, K. Leininger, and A.R. Smith, *ibid.* **38**, 1722 (1988); J.C. Hill, F.K. Wohn, J.A. Winger, M. Khayat, M.T. Mercier, and A.R. Smith, *ibid.* **39**, 524 (1989); J.C. Hill and F.K. Wohn, *ibid.* **39**, 2474 (1989).

[2] J.D. Jackson, *Classical Electrodynamics* (Wiley, New York, 1975), p. 520.

[3] J.C. Hill, F.K. Wohn, D.D. Schwellenbach, and A.R. Smith, Phys. Lett. B **273**, 371 (1991).

[4] C.A. Bertulani and G. Baur, Phys. Rep. **163**, 299 (1988).

[5] W.J. Llope and P. Braun-Munzinger, Phys. Rev. C **41**, 2644 (1990).

[6] W.J. Llope and P. Braun-Munzinger, Phys. Rev. C **45**, 799 (1992).

[7] C. Ziegler, T. Brohm, H.-G. Clerc, H. Geissel, K.-H. Schmidt, K. Sümmerer, D. Vieira, and B. Voss, GSI Scientific Report GSI-91-1, 291, 1991.

[8] Y. Yariv and Z. Fraenkel, Phys. Rev. C **20**, 2227 (1979).

[9] S.B. Kaufman and E.P. Steinberg, Phys. Rev. C **22**, 167 (1980).

[10] J.W. Norbury, Phys. Rev. C **41**, 372 (1990); **42**, 711 (1990).

[11] F.E. Bertrand, Annu. Rev. Nucl. Sci. **26**, 457 (1976).

[12] B.L. Berman, At. Data Nucl. Data Tables **15**, 319 (1975); A. Veyssière, H. Beil, R. Bergère, P. Carlos, and A. Leprêtre, Nucl. Phys. **A159**, 561 (1970).

[13] B.L. Berman, R.E. Pywell, S.S. Dietrich, M.N. Thompson, K.G. McNeill, and J.W. Jury, Phys. Rev. C **36**, 1286 (1987).

[14] GSI version of the code ALICE [M. Blann and F. Plasil, Phys. Rev. Lett. **29**, 303 (1972)]; W. Reisdorf and M. Schädel, Z. Phys. A **343**, 47 (1992).

[15] C.J. Benesh, B.C. Cook, and J.P. Vary, Phys. Rev. C **40**, 1198 (1989).

[16] S. Kox, A. Gamp, C. Perrin, J. Arvieux, R. Bertholet, J.F. Bruandet, M. Buenerd, R. Cherkaoui, A.J. Cole, Y. El-Masri, N. Longequeue, J. Menet, F. Merchez, and J.B. Viano, Phys. Rev. C **35**, 1678 (1987).

[17] R. Schmidt, Th. Blaich, Th.W. Elze, H. Emling, H. Freiesleben, K. Grimm, W. Henning, R. Holzmann, J.G. Keller, H. Klingler, R. Kulessa, J.V. Kratz, D. Lambrecht, J.S. Lange, Y. Leifels, E. Lubkiewicz, E.F. Moore, E. Wajda, W. Prokopowicz, Ch. Schütter, H. Spies, K. Stelzer, J. Stroth, W. Walus, H.J. Wollersheim, M. Zinser, and E. Zude, LAND Collaboration, GSI Report GSI-92-64, 1992 (submitted to Phys. Rev. Lett.).